

## Large thermopower anisotropy in PdCoO<sub>2</sub> thin films

P. Yordanov<sup>1</sup>,<sup>\*</sup> W. Sigle,<sup>1</sup> P. Kaya,<sup>1</sup> M. E. Gruner,<sup>2</sup> R. Pentcheva,<sup>2</sup> B. Keimer,<sup>1</sup> and H.-U. Habermeier<sup>1,\*</sup>

<sup>1</sup>Max-Planck Institute for Solid State Research, 70569 Stuttgart, Germany

<sup>2</sup>Theoretical Physics and Center for Nanointegration (CENIDE), University of Duisburg-Essen, 47057 Duisburg, Germany



(Received 12 June 2019; published 15 August 2019)

Motivated by recent theoretical studies predicting a large thermopower anisotropy in the layered delafossite PdCoO<sub>2</sub>, we have used pulsed laser deposition to synthesize thin films on (0001)-oriented and offcut Al<sub>2</sub>O<sub>3</sub> substrates. By combining transport measurements on films with different offcut angles, tensor rotation relations, and an iterative fit procedure for the transport parameters, we have determined the resistivity and the thermopower along the main crystallographic axes in the temperature range 300–815 K. The data reveal a small positive Seebeck coefficient along the delafossite planes and a large negative Seebeck coefficient perpendicular to the planes, in excellent agreement with density functional calculations in the presence of moderate Coulomb correlations. The methodology introduced here is generally applicable for measurements of the thermoelectric properties of materials with highly anisotropic electronic structures.

DOI: [10.1103/PhysRevMaterials.3.085403](https://doi.org/10.1103/PhysRevMaterials.3.085403)

### I. INTRODUCTION

Since the discovery of several new delafossite compounds by Shannon *et al.* in 1971 [1], PdCoO<sub>2</sub> has attracted growing attention due to its unusual electric transport properties. Its layered crystal structure comprises highly conducting Pd (Pd<sup>1+</sup>, 4d<sup>9</sup>) and insulating CoO<sub>6</sub> (Co<sup>3+</sup>, 3d<sup>6</sup>) blocks arranged on triangular lattices [Fig. 1(b)] [2,3]. Recent transport experiments have revealed a remarkably low in-plane resistivity  $\rho_{ab}$ , a  $\rho_c/\rho_{ab}$  anisotropy of more than two orders of magnitude [4], colossal magnetoresistance effects [5,6], and hydrodynamic contributions to the electric transport [7]. Furthermore, two recent theoretical studies based on first principles and Boltzmann transport theory calculations have predicted a highly anisotropic Seebeck coefficient with opposite signs parallel and perpendicular to the planes [8,9]. However, these results are still lacking experimental confirmation, because the limited size of the available single crystals along the *c* axis does not allow reliable thermopower measurements. Materials that exhibit such large anisotropies in the thermopower are rare and could enable the design of thermoelectric devices. Of particular interest are generators and heat sensors that make use of the transverse Seebeck effect, where the temperature gradient and the generated electric potential are noncollinear [10,11].

By using pulsed laser deposition (PLD), we have synthesized PdCoO<sub>2</sub> thin films on normal and offcut Al<sub>2</sub>O<sub>3</sub> (0001) substrates, with the main objective to measure the in-plane ( $S_{ab}$ ) and *c* axis ( $S_c$ ) Seebeck coefficients at high temperatures. Ideally, a single defect-free, perfectly oriented thin film deposited on an offcut substrate with accessible *c*-axis component should be sufficient to obtain the resistivity and Seebeck coefficient along the main axes. However, in practice, these conditions are difficult to meet. Our transport

measurements revealed that all PdCoO<sub>2</sub> thin films are influenced by defects, most likely from grain boundaries, resulting in substantially higher resistivity and reduced residual resistivity ratios compared to bulk single crystals [12]. For the thin films on offcut substrates, the situation is more complex because the step-terrace structure introduces additional scattering channels from imperfections in the crystallite orientation such as uncontrolled rotations and/or twin growth. These latter factors can lead to mixed responses and significant errors in the data evaluation even for the thermopower, which is normally much less sensitive to defects than the electrical conductivity. In an attempt to minimize these uncertainties, we follow a scheme that involves measurements of four types of thin films; one deposited on a normal planar substrate that serves as a reference for  $\rho_{ab}$  and  $S_{ab}$ , and films deposited on substrates with three different offcut angles. By applying tensor rotation relations and an iterative fit procedure to the data along the offcut direction ( $\rho_{ab/c}$ ,  $S_{ab/c}$ ), we obtain the *c*-axis quantities  $\rho_c$  and  $S_c$ . The results for the Seebeck coefficient are in excellent agreement with density functional theory calculations with a moderate Hubbard parameter combined with Boltzmann transport theory, and fully support the main features obtained in previous experimental and theoretical studies [8,9,13]. The thermopower anisotropy in the PdCoO<sub>2</sub> thin films could thus stimulate further research on thermoelectric devices.

### II. THIN FILM DEPOSITION AND BASIC CHARACTERIZATION

PdCoO<sub>2</sub> films of thickness 8–15 nm were prepared by PLD on normal planar (offcut angle  $\theta = 0^\circ$ ) Al<sub>2</sub>O<sub>3</sub> (0001) substrates, and substrates that were nominally offcut by  $\theta = 5^\circ, 10^\circ$ , and  $20^\circ$  towards (11-20). Prior to deposition, the substrates were cleaned in an ultrasonic bath with a mixture of ethanol and acetone. A stoichiometric PdCoO<sub>2</sub> target and a large range of oxygen pressures between 0.2 and 2.3 mbar,

\*Deceased.

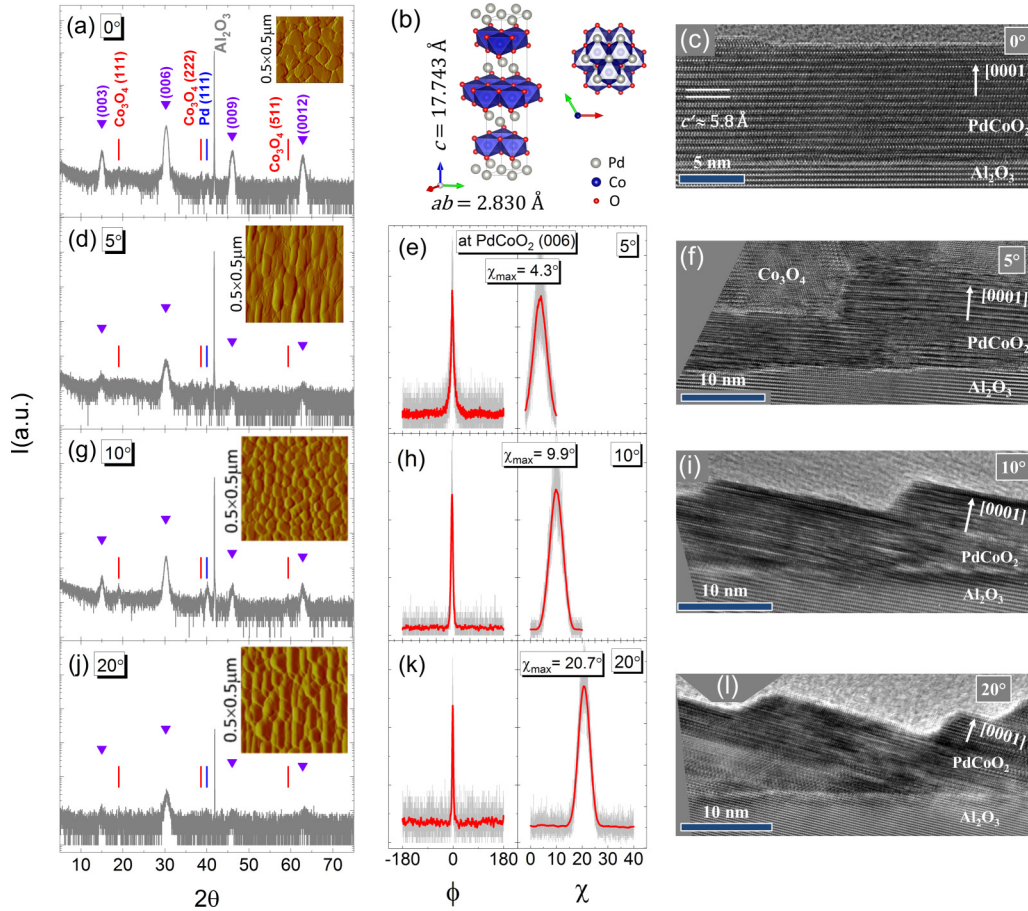


FIG. 1. XRD patterns of PdCoO<sub>2</sub> thin films on (a) 0° planar and nominally (d) 5° (g) 10°, and (j) 20° offcut Al<sub>2</sub>O<sub>3</sub> (0001) substrates. Reflections due to residual Pd and Co<sub>3</sub>O<sub>4</sub> inclusions are also marked. Insets: AFM images. (b) PdCoO<sub>2</sub> delafossite crystal structure [1] (Visualization program - VESTA 3) (e), (h), and (k) φ and χ scans taken at the PdCoO<sub>2</sub> (006) Bragg reflection showing the c-axis azimuthal orientation and the actual film offcut angle θ = χ<sub>max</sub>. Solid lines represent averaged data. (c), (f), (i), and (l) cross-sectional HRTEM images of PdCoO<sub>2</sub> thin film on nominally 0°, 5°, 10°, and 20° offcut Al<sub>2</sub>O<sub>3</sub> (0001) substrates. Solid lines denote the Pd-Pd interlayer spacing c' = c/3, indicating up to ~2 % c-axis unit cell compression with respect to the bulk lattice constant 17.743/3 = 5.914 Å.

with an addition of ~10 % argon, were used in exploratory synthesis experiments. The substrate temperature was kept in the range ~620–625°C. After deposition, the gas flow was cut and the samples were cooled in vacuum. High-oxygen-pressure conditions (2–2.3 mbar) combined with a laser energy density of ~1.9 J/cm<sup>2</sup> and a repetition rate of 3 Hz, resulted in a growth rate of ~0.01 Å/pulse, minimal Pd and Co<sub>3</sub>O<sub>4</sub> secondary phase inclusions, and optimal film crystallinity.

This was verified by x-ray diffraction (XRD) patterns, as well as atomic force microscopy (AFM) [Figs. 1(a), 1(d), 1(g), and 1(j)] and high-resolution transmission electron microscopy (HRTEM) images [Figs. 1(c), 1(f), 1(i), and 1(l)]. We note that trace amounts of Co<sub>3</sub>O<sub>4</sub> were found primarily in the form of disconnected patches on the films surfaces.

### III. RESISTIVITY AND SEEBECK COEFFICIENT RESULTS

The upper panels of Fig. 2 represent resistivity and Seebeck coefficient data for thin films on 0° (planar), 5°, 10°, and 20° offcut substrates in the temperature ranges 4–815 K and

300–815 K, respectively. In the low-temperature range, 4–300 K, the resistivity was measured by a homebuilt device placed in a helium dewar, while at high-temperatures, 300–815 K, both resistivity and Seebeck coefficient were measured simultaneously in complete heating-cooling cycles by utilizing an ULVAC ZEM3 system equipped with Pt electrodes. The measurements were performed in a helium atmosphere with ~1 % oxygen and a total pressure of 950 mbar in order to ensure the thermal stability of the PdCoO<sub>2</sub> thin films at higher temperatures. All measurements were conducted in a four-point inline contact configuration according to the sketch given in the lower panel of Fig. 2(a). Perpendicular to the offcut direction, they ideally yield the in-plane quantities ρ<sub>ab</sub> and S<sub>ab</sub>, and along the offcut direction they yield ρ<sub>ab/c</sub> and S<sub>ab/c</sub>, with a c-axis component that depends on the offcut angle. In the absence of defects, the c-axis quantities ρ<sub>c</sub> and S<sub>c</sub> can be obtained by measuring a single thin-film sample deposited on a substrate with a nonzero offcut angle θ and by applying the tensor rotation relations:

$$\rho_c = (\rho_{ab/c} - \rho_{ab} \times \cos^2\theta) / \sin^2\theta, \quad (1)$$

$$S_c = (S_{ab/c} - S_{ab} \times \cos^2\theta) / \sin^2\theta, \quad (2)$$

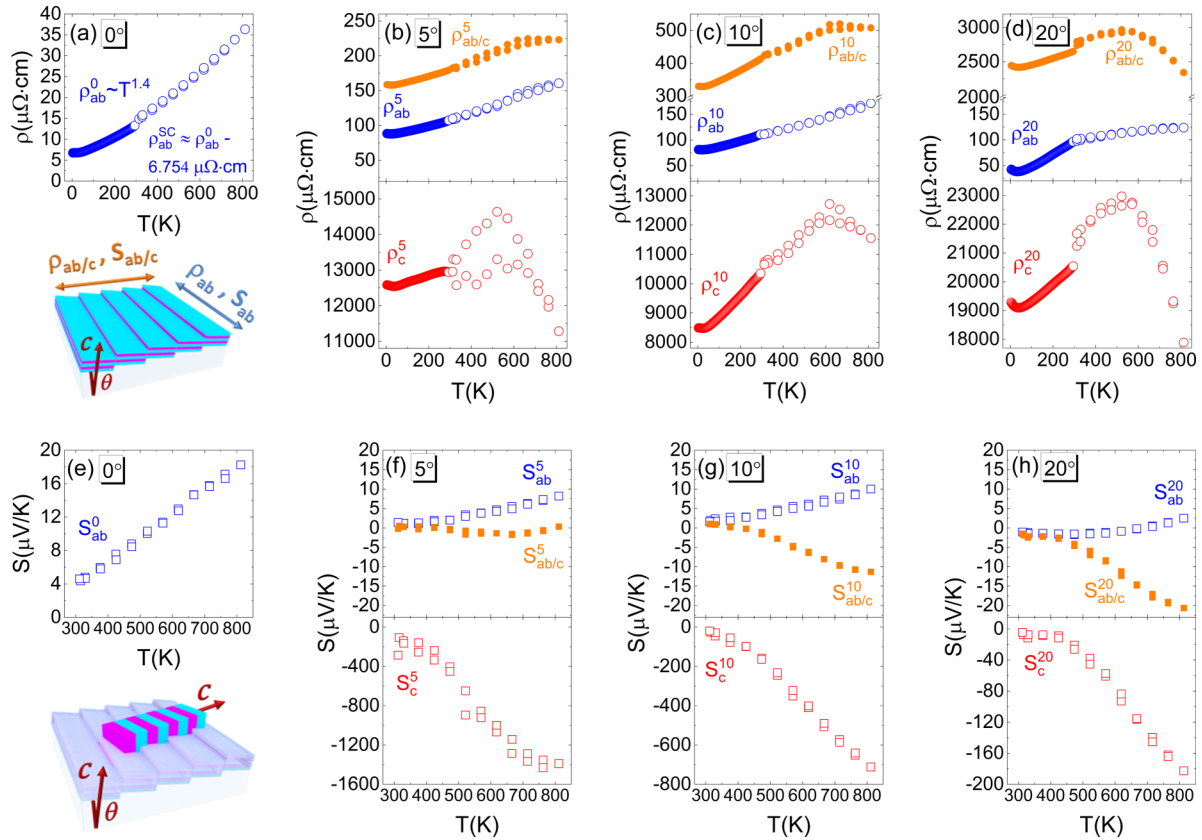


FIG. 2. Experimental in-plane and offcut direction resistivity  $\rho_{ab}$ ,  $\rho_{ab/c}$  (4–815 K) (a), (b), (c), and (d) (upper panels), and Seebeck coefficient  $S_{ab}$ ,  $S_{ab/c}$  (300–815 K) (e), (f), (g), and (h) (upper panels) data for films with  $0^\circ$ ,  $5^\circ$ ,  $10^\circ$ , and  $20^\circ$  offcut substrates, respectively. The calculated  $c$  axis  $\rho_c$  and  $S_c$  for films on  $5^\circ$ ,  $10^\circ$ , and  $20^\circ$  are given in the lower panels. In the calculation, the actual offcut angles as obtained from the XRD  $\chi_{\max}$  analysis were used:  $4.3^\circ$ ,  $9.9^\circ$ , and  $20.7^\circ$ . Lower panel of figure (a) depicts the experimental setup for resistivity and Seebeck coefficient measurements. For offcut angle samples, two consecutive measurements, perpendicular and parallel to the offcut direction yield  $\rho_{ab}$ ,  $S_{ab}$  and  $\rho_{ab/c}$ ,  $S_{ab/c}$ , respectively. Lower panel of figure (e) represents an effective-medium model sketch for the defect contribution from PdCoO<sub>2</sub> crystallites with the  $c$  axis inclined at angle larger than the offcut one and rotated in-plane.

where the final result must be identical for all offcut angles. The evaluated  $c$ -axis resistivity  $\rho_c$  and Seebeck coefficient  $S_c$ , for the PdCoO<sub>2</sub> films on  $5^\circ$ ,  $10^\circ$  and  $20^\circ$  substrates are given in the lower panels of Fig. 2. Focusing first on the  $0^\circ$  thin film data, we notice that the in-plane resistivity in the low-temperature range  $\rho_{ab}^0(4\text{--}300\text{ K}) \sim 6\text{--}12\ \mu\Omega\text{ cm}$ , with a residual resistivity ratio of  $\sim 2$ , is much larger compared to that of single crystals, where typically  $\rho_{ab}(4\text{--}300\text{ K}) \sim 0.008\text{--}7\ \mu\Omega\text{ cm}$  is obtained [4,12]. On the other hand, a closer analysis of our planar thin film samples revealed that the temperature dependence in the range 50–300 K, as well as for the extended range 50–815 K, can be reliably fitted by a power-law exponent identical to the one for PdCoO<sub>2</sub> single crystals  $\rho_{ab} \sim T^{1.4}$  [12]. This peculiar temperature dependence, which is between that of a simple metal and a correlated-electron system, was attributed to scattering from high-frequency phonon modes. Comparison with the thin film data showed that the single crystal temperature-dependent in-plane resistivity is nearly fully recovered by subtracting a constant contribution; see Fig. 2(a).

Taking into account the above arguments, and recalling the very similar results reported for the PdCoO<sub>2</sub> thin film resistivity by Harada *et al.* [14], where no secondary phases were evident in the XRD, we can conclude that the trace

amount of impurities we encounter does not noticeably modify the transport properties in our samples. Further, the higher resistivity in the PdCoO<sub>2</sub> thin films compared to single crystals is mainly due to grain boundary scattering, which adds a temperature-independent contribution. As grain boundary formation in heteroepitaxial thin films is difficult to avoid (see also AFM images, insets in Fig. 1), this situation limits the capability of thin-film technology to explore the highly conductive properties of PdCoO<sub>2</sub> on large area samples. In the following, the results from the  $0^\circ$  film [Figs. 2(a) and 2(e)] will serve as reference for the in-plane resistivity  $\rho_{ab}^0$  and Seebeck coefficient  $S_{ab}^0$ . In the high-temperature range,  $\rho_{ab}^0$  does not show any anomalies, and the superlinear increase remains unchanged up to the highest measured temperature of 815 K. As the thermopower is not sensitive to grain boundary scattering, we can expect  $S_{ab}^0$  to be even closer to the in-plane thermopower of single-crystalline PdCoO<sub>2</sub> unless other factors, such as strain, influence the results. Indeed, the high-temperature measurements of  $S_{ab}^0$ , Fig. 2(e), reveal small metallic-like positive values with a weak superlinear (rather than strictly linear) temperature dependence that increases from  $4\ \mu\text{V/K}$  at room temperature to  $18\ \mu\text{V/K}$  at 815 K, in excellent agreement with the theoretical studies [8,9].

In the films on offcut substrates [Figs. 2(b)–2(d)] the temperature dependent in-plane resistivity shows similar behavior ( $\rho_{ab}^5, \rho_{ab}^{10}, \rho_{ab}^{20}$  (4 – 815 K)  $\sim 50 - 150 \mu\Omega \text{ cm}$ ), but with values considerably larger compared to those of the film on the planar substrate. As expected from the highly anisotropic electronic structure of PdCoO<sub>2</sub>, the resistivity along the offcut directions containing the *c*-axis component ( $\rho_{ab/c}^5, \rho_{ab/c}^{10}, \rho_{ab/c}^{20}$ ) is much larger. It increases monotonically upon heating to  $\sim 600$  K and then saturates and exhibits a tendency to decrease, which is clearly visible in the *c*-axis parameters  $\rho_c^5, \rho_c^{10}$  and  $\rho_c^{20}$  calculated using Eq. (1). However, from the *c*-axis resistivity plots, it is obvious that the absolute values computed in this way deviate substantially from those reported for single crystals  $\rho_c(4-300 \text{ K}) \sim 3-1000 \mu\Omega \text{ cm}$  [12]. They also differ substantially from sample to sample, whereas identical results (within the experimental error) are expected for all samples along the main crystallographic axes:  $\rho_{ab} \equiv \rho_{ab}^5 \approx \rho_{ab}^{10} \approx \rho_{ab}^{20}$  and  $\rho_c \equiv \rho_c^5 \approx \rho_c^{10} \approx \rho_c^{20}$ . The trend found in the temperature-dependent Seebeck coefficient for the three offcut angle samples [Figs. 2(f)–2(h)] is analogous to that for the resistivity, but with opposite sign. The in-plane coefficients  $S_{ab}^5, S_{ab}^{10}$ , and  $S_{ab}^{20}$  measured in the films on offcut substrates are lower than the one in the film on the planar substrate  $S_{ab}^0$ . Along the offcut direction,  $S_{ab/c}^5, S_{ab/c}^{10}$ , and  $S_{ab/c}^{20}$  progressively deviate from the in-plane coefficient upon heating, indicating a large anisotropy also in the thermopower. Above  $\sim 600$  K the Seebeck coefficients with *c*-axis component show a tendency to saturate. Using Eq. (2) to compute the Seebeck coefficient along the *c*-axis, we obtain a very large negative, but variable result for  $S_c$ . Obviously, the Seebeck coefficients for both in-plane and *c*-axis directions do not fulfill the conditions:  $S_{ab} \equiv S_{ab}^5 \approx S_{ab}^{10} \approx S_{ab}^{20}$  and  $S_c \equiv S_c^5 \approx S_c^{10} \approx S_c^{20}$ . The measured resistivity and Seebeck coefficient for the two directions thus seem to be influenced by additional terms of higher resistivity and negative Seebeck coefficient, which very likely arise from regions with crystallites where the *c*-axis is inclined at an angle larger than the offcut angle and further rotated in-plane. Although the  $\phi$  and  $\chi$  scans shown in Figs. 1(e), 1(h), and 1(k) indicate excellent macroscopic orientation along the offcut direction, the formation of misaligned domains cannot be excluded especially in view of the large area of the films ( $10 \times 10 \text{ mm}^2$ ), and of additional factors such as strain and the step-terrace morphology of the offcut substrates. The lower panel of Fig. 2(e) represents an effective-medium model sketch of a possible defected region leading to *c*-axis self-contamination. In general, these regions can have random spatial distribution with uncontrolled rotation angles, form nonrandom patterns along the thin film with gradual angular changes, or exhibit mesoscopic textures such as twins. It turns out, however, that the situation realized in our films allows a straightforward analysis from which consistent values for the in-plane and out-of-plane Seebeck coefficients can be derived.

#### IV. CORRECTION PROCEDURE AND COMPARISON TO THEORY

From the data on offcut samples presented in Figs. 2(b)–2(d) and 2(f)–2(h) it is clear that a correction procedure that

eliminates the defect contributions (or minimizes them to a satisfactory level) is required to obtain consistent results. To begin with, let us suppose that the response along each direction, in-plane and offcut, can be divided into the following terms:  $\rho_{ab}^\theta, S_{ab}^\theta$  (which include the in-plane response  $\rho_{ab}, S_{ab}$  and a defect contribution  $\rho_{ab}^{\text{def}}, S_{ab}^{\text{def}}$ ), and  $\rho_{ab/c}^\theta, S_{ab/c}^\theta$  (which consist of  $\rho_{ab}, S_{ab}$ , a defect term  $\rho_{ab/c}^{\text{def}}, S_{ab/c}^{\text{def}}$  and the *c*-axis  $\rho_c, S_c$  components with relative weight that depends on the offcut angle). This breakdown is justified by the results from the  $\phi$  and  $\chi$  scans [Figs. 1(e), 1(h), and 1(k)] showing that at least a large fraction of the crystallites is correctly aligned. As for the defect terms along the in-plane and along the offcut direction, they are generally not identical, i.e.,  $\rho_{ab}^{\text{def}}, S_{ab}^{\text{def}} \neq \rho_{ab/c}^{\text{def}}, S_{ab/c}^{\text{def}}$ , which is where the problems with the calculation of the *c* axis [Eqs. (1) and (2)] arise. The nonzero difference between the two defect terms is enhanced by the  $\sin^2\theta$  term in the denominator thereby generating unreasonably large errors. A correction procedure for the in-plane response  $\rho_{ab}^\theta, S_{ab}^\theta$  is not of great concern since we can use the reference from the thin film on the planar  $0^\circ$  substrate  $\rho_{ab}^0, S_{ab}^0$  [Eq. (3)]. For the offcut direction, this is not the case and we need to subtract the defect term from  $\rho_{ab/c}^\theta, S_{ab/c}^\theta$  for all offcut films. A possible way to do this is to construct an appropriate test function [Eq. (4), left parentheses], which we can compare by fitting to the defect term until they become equal and eventually cancel each other. The iteration continues until the corrected quantities  $\rho_{ab}^{\theta \text{ corr}}, S_{ab}^{\theta \text{ corr}}$  and  $\rho_{ab/c}^{\theta \text{ corr}}, S_{ab/c}^{\theta \text{ corr}}$ , inserted again in Eqs. (1) and (2), return equal results (within reasonable limits) for the *c*-axis parameters  $\rho_c, S_c$  [condition in Eq. (5)], simultaneously for at least three samples with different offcut angles. In this way, the correction procedure for the resistivity  $\rho$  and Seebeck coefficient  $S$  can be summarized by the following equations for the two directions:

$$\begin{aligned} \rho_{ab}^{\theta \text{ corr}}, S_{ab}^{\theta \text{ corr}} &\equiv \rho_{ab}^0, S_{ab}^0 \equiv \rho_{ab}, S_{ab}, \\ \rho_{ab/c}^{\theta \text{ corr}}, S_{ab/c}^{\theta \text{ corr}} &= \rho_{ab/c}^\theta, S_{ab/c}^\theta \\ &\quad - [(\rho_{ab/c}^\theta, S_{ab/c}^\theta - \rho_{ab}^0, S_{ab}^0 \cdot \cos^2 \theta) \\ &\quad \times \cos^2(C_{\rho, S}^{\text{fit}} \cdot \theta)], \end{aligned} \quad (3)$$

$$\begin{aligned} C_{\rho, S}^{\text{fit}} \text{ until } \{ \rho_{ab}^{\theta \text{ corr}}, S_{ab}^{\theta \text{ corr}}, \rho_{ab/c}^{\theta \text{ corr}}, S_{ab/c}^{\theta \text{ corr}} \} \\ \rightarrow \{ \text{Eqs. (1), (2)} \} \rightarrow \{ \rho_c^\theta, S_c^\theta \} \cong \rho_c, S_c. \end{aligned} \quad (5)$$

The representation of the fit parameter as  $\cos^2(C_{\rho, S}^{\text{fit}} \cdot \theta)$  is written such that the dependence on the offcut angle is explicit. By applying the iterative fit procedure described above to the data for the offcut films, we obtained consistent results for the resistivity and Seebeck coefficient with two fit parameters  $C_{\rho}^{\text{fit}} = 88$  and  $C_S^{\text{fit}} = 3$ , respectively, which are identical for all three samples  $5^\circ, 10^\circ$ , and  $20^\circ$ . These results indicate the presence of nonrandom defects with density proportional to the offcut angle that mix the in-plane and out-of-plane response functions. The results are presented in Figs. 3(a)–3(d). For a more detailed description of the fit procedure, see the Supplementary Material [15].

Figure 3(a) shows that the corrected resistivity  $\rho_{ab/c}^{\theta \text{ corr}}$  exhibits a systematic increase as a function of the offcut angle, as expected, and that the *c*-axis response determined in this

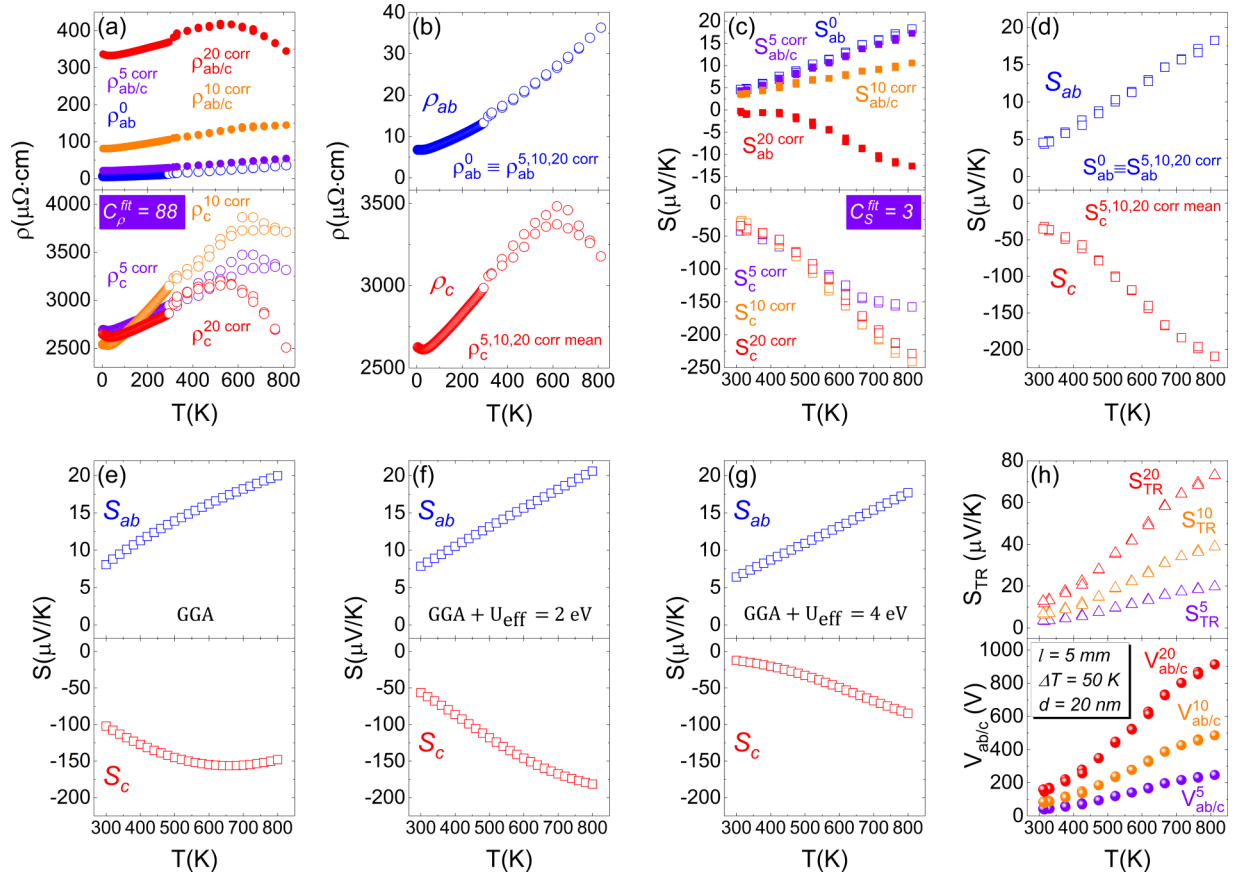


FIG. 3. (a) and (c) Corrected in-plane  $\rho_{ab}$ ,  $S_{ab} \equiv \rho_{ab}^{\theta \text{ corr}}$ ,  $S_{ab}^{\theta \text{ corr}} \equiv \rho_{ab}^0$ ,  $S_{ab}^0$ , offcut direction  $\rho_{ab/c}^{\theta \text{ corr}}$ ,  $S_{ab/c}^{\theta \text{ corr}}$  (upper panels), and the corresponding  $c$ -axis  $\rho_c$ ,  $S_c \equiv \rho_c^{\theta \text{ corr}}$ ,  $S_c^{\theta \text{ corr}}$  (lower panels) resistivity (4–815 K) and Seebeck coefficient (300–815 K), (b) and (d) display the in-plane and the  $c$ -axis ( $c$ -axis averaged) results only, (e), (f), and (g) model Seebeck coefficient for different effective on-site Coulomb repulsion energies:  $U_{\text{eff}} = 0, 2, \text{ and } 4 \text{ eV}$ . The calculations were performed by a combination of first-principles DFT and semiclassical Boltzmann transport theory. Static electronic correlation effects on the Co  $3d$  states were taken into account by applying the (GGA +  $U$ ) scheme. Further technical details can be found in Ref. [9]. (h) Transverse Seebeck coefficient (upper panel) and calculated laser induced transverse voltage (lower panel) for the three different offcut angles  $\theta = 5^\circ, 10^\circ, \text{ and } 20^\circ$ . The parameters used in the calculation are given in the inset.

way is in a very reasonable range. For clarity, the results for the main axes only,  $\rho_{ab} \equiv \rho_{ab}^{\theta \text{ corr}} \equiv \rho_{ab}^0$  and the averaged  $\rho_c \equiv \rho_c^{\theta \text{ corr mean}}$ , are shown in a separate plot [Fig. 3(b)]. Unlike the in-plane resistivity  $\rho_{ab}$ ,  $\rho_c$  exhibits a large residual contribution and an upturn visible at low temperatures. This is not surprising since the specific terrace structure along the offcut direction implies a step-flow growth mechanism and conditions for the formation of various defects such as stacking faults, antiphase boundaries, accumulation of vacancies and impurities, and additional strain effects [16], all of which can act as localization centers.

As already discussed in Sec. III, the in-plane resistivity follows the superlinear trend  $\rho_{ab} \sim T^{1.4}$  in a very wide temperature range (50–815 K), while the temperature dependence of the  $c$ -axis resistivity (50–600 K) is closer to linear, which is also consistent with the data for PdCoO<sub>2</sub> single crystals where  $\rho_c \sim T^{1.05}$  has been reported [12]. Above  $\sim 600$  K,  $\rho_c$  reaches saturation followed by a downturn. It is difficult to assess whether this is a crossover to an activated regime, with an activation energy of approximately  $E_a \approx 50$  meV, or due the approach of the Mott-Ioffe-Regel (MIR) resistivity limit.

We note, however, that similar behavior in the temperature-dependent resistivity is also observed in other layered materials such as Sr<sub>2</sub>RuO<sub>4</sub> and NaCo<sub>2</sub>O<sub>4</sub> [17, 18]. We also recall that Ong *et al.* [8] expected the MIR limit for the  $c$  axis in PdCoO<sub>2</sub> at temperatures around  $\sim 870$  K, corresponding to  $\rho_c \sim 3000 \mu\Omega\text{cm}$  in single crystals. This estimate matches fairly well the  $c$ -axis resistivity values at the maximum obtained in our films. On the other hand, experimental magnetoresistance data showed an interlayer hopping energy of  $t_c \approx 17$  meV and a loss of coherence in the  $c$ -axis direction at temperature as low as  $\sim 90$  K [6, 19]. These findings bring about many open questions related to the electric and thermoelectric transport properties in the incoherent transport regime, where the resistivity is comparable to the MIR limit, that is, when the charge carriers mean free path becomes comparable to the  $c$ -axis interlayer spacing. Since in this case the uncertainty in the electron wave vector is of the order of the Brillouin zone size, a semiclassical transport theory description becomes questionable. Electron correlations further contribute to the complexity of models for transport phenomena in this regime [20–22].

Compared to the resistivity, the thermopower is much less sensitive to typical thin film defects, and we can expect that the corrections here are more modest and predominantly due to  $c$ -axis misalignment. After applying the correction procedure to the Seebeck coefficient, we indeed obtain a consistent gradual decrease with the offcut angle for  $5^\circ$ ,  $10^\circ$ , and  $20^\circ$ , and closely matching results for the  $c$ -axis response [Fig. 3(c)]. In the temperature range 300–815 K, for the main axes  $S_{ab} \equiv S_{ab}^{\theta \text{ corr}} \equiv S_{ab}^0$  and  $S_c \equiv S_c^{\theta \text{ corr mean}}$  [Fig. 3(d)], we obtain  $S_{ab} \sim 4 - 18 \mu\text{V/K}$  and  $S_c \sim (-30) - (-200) \mu\text{V/K}$ . These findings are consistent with the main features predicted in the theoretical studies, that is, small metallic-like positive in-plane and large semiconductor-like negative  $c$ -axis Seebeck coefficients [8,9]. To gain more insight into the underlying transport mechanisms in PdCoO<sub>2</sub>, we have compared our thermopower data with calculations of the temperature-dependent Seebeck coefficient in the framework of density functional theory (DFT) in the generalized gradient approximation (GGA) without a Hubbard  $U$  parameter, and for two different effective  $U$  values at the Co site,  $U_{\text{eff}} = 0, 2, \text{ and } 4 \text{ eV}$ , Figs. 3(e)–3(g). The best overall agreement is obtained for  $U_{\text{eff}} = 2 \text{ eV}$ , indicating that modest corrections to the GGA are necessary to account for electronic correlations. The in-plane  $S_{ab}$  compares equally well for  $U_{\text{eff}} = 4 \text{ eV}$ , and to the result obtained by Ong *et al.* [8], where no additional correlations had been taken into account. Considering the experimental error and the possible influence of epitaxial strain [as indicated from the TEM image in Fig. 1(c)], it is obvious that the experimental results do not discriminate between the different predictions for  $S_{ab}$ . On the other hand, the presence of Co  $3d$  states in the vicinity of the Fermi level is relevant for the out-of-plane transport [8,9]. With increasing  $U_{\text{eff}}$ , these states are pushed away from the Fermi level, and the  $c$ -axis Seebeck coefficient  $S_c$  is strongly affected as can be seen in the lower panels of Figs. 3(e)–3(g).

Finally, based on the main axes Seebeck coefficients [Fig. 3(d)] we can calculate the temperature-dependent transverse Seebeck coefficient,  $S_{\text{TR}}$ , as well as the voltage  $V_{ab/c}$  that could potentially be generated in the thin films by laser illumination, the so-called laser-induced transverse voltage effect (LITV) [11]:

$$S_{\text{TR}} = \frac{1}{2} \sin 2\theta (S_{ab} - S_c), \quad (6)$$

$$\begin{aligned} V_{ab/c} &= \frac{l}{d} \Delta T_z S_{\text{TR}}, \\ V_{ab} &= 0, \end{aligned} \quad (7)$$

where  $V_{ab/c}$  and  $V_{ab}$  are the voltages along the offcut and the in-plane direction of the film,  $l$  is the laser spot length at the film surface,  $\Delta T_z$  is the temperature difference between the illuminated front side and the back side of the film, and  $d$  is the film thickness. As evident from the lower panel of Fig. 3(h), the generated voltages can be significant. For example, by assuming typical parameters for LITV experiments:  $l = 5 \text{ mm}$ ,  $\Delta T = 50 \text{ K}$ , and  $d = 20 \text{ nm}$ , we estimate  $V_{ab/c} \approx 36, 72, \text{ and } 134 \text{ V}$  at room temperature for  $\theta = 5^\circ, 10^\circ, \text{ and } 20^\circ$ , respectively. However, because of the above described tendency of offcut PdCoO<sub>2</sub> films to form domains

with a misoriented  $c$  axis, the LITV signal can mix along the two directions,  $V_{ab} \neq 0$ , and therefore may be lower than predicted by Eqs. (6) and (7) in real experiments.

## V. CONCLUSIONS

In conclusion, utilizing the PLD technique we have successfully synthesized PdCoO<sub>2</sub> thin films on  $0^\circ$  planar,  $5^\circ$ ,  $10^\circ$ , and  $20^\circ$  offcut Al<sub>2</sub>O<sub>3</sub> (0001) substrates. These films allowed us to experimentally determine the high-temperature (300–815 K) transport properties along the main crystallographic directions. The films on planar substrates yielded high-quality reference data for the in-plane resistivity and Seebeck coefficient. The films on offcut substrates, on the other hand, revealed substantial mixing of in-plane and out-of-plane response functions, presumably due to regions of misoriented crystallites with  $c$  axes inclined at angles larger than the offcut ones and further rotated in the in-plane direction. By applying the tensor rotation relations and an iterative fit procedure to the data for the offcut samples, we were able to obtain consistent results for both the resistivity and the Seebeck coefficient along the  $c$  axis. In the temperature range 300–815 K, we obtained  $S_{ab} \sim 4 - 18 \mu\text{V/K}$  and  $S_c \sim (-30) - (-200) \mu\text{V/K}$ , for the in-plane and  $c$ -axis direction, respectively, which demonstrates excellent overall agreement with existing theoretical studies. Furthermore, detailed comparison to model calculations of the Seebeck coefficient where an effective on-site Coulomb repulsion energy was included indicate that moderate electron-electron correlations are relevant and should be taken into account to adequately describe the thermopower in PdCoO<sub>2</sub>. The main axes electric and thermoelectric transport quantities obtained here with the correction procedure may be used in the description of polycrystalline PdCoO<sub>2</sub>, with appropriate modifications accounting for the random crystallite orientation. The outcome of the effective model description of polycrystalline PdCoO<sub>2</sub> (as well as of other materials and thin-film systems) will determine the range of applicability of our methodology. From the practical point of view, the large thermopower anisotropy and the good thermal stability qualify PdCoO<sub>2</sub> thin films as promising candidates for thermoelectric devices such as laser sensors, where the signal level depends on the difference  $\Delta S = S_{ab} - S_c$ . Further interesting perspectives include thin-film structures with tunable angle-dependent power factor,  $P = S^2/\rho$ , which take advantage of the metallic in-plane conductivity and the large semiconductor-like  $c$ -axis Seebeck coefficient confirmed in our experiments.

## ACKNOWLEDGMENTS

We acknowledge financial support by the Deutsche Forschungsgemeinschaft (DFG, German Research Foundation) – Project No. 107745057 - CRC/TRR 80, subproject G8; Project No. 278162697 - CRC 1242, subproject C02, and partial support by Coherent Inc., Wilsonville, OR (USA). The authors are indebted to A. S. Gibbs, S. Prill-Diemer, Y. Krockenberger, S. Schmid, B. Lemke, G. Cristiani, B. Stuhlhofer, G. Logvenov, U. Salzberger and Ina Georgieva for experimental support, advice, and discussions.

- [1] R. D. Shannon, D. B. Rogers, and C. T. Prewitt, *Inorg. Chem.* **10**, 713 (1971).
- [2] K. P. Ong, J. Zhang, J. S. Tse, and P. Wu, *Phys. Rev. B* **81**, 115120 (2010).
- [3] A. P. Mackenzie, *Rep. Prog. Phys.* **80**, 032501 (2017).
- [4] C. W. Hicks, A. S. Gibbs, A. P. Mackenzie, H. Takatsu, Y. Maeno, and E. A. Yelland, *Phys. Rev. Lett.* **109**, 116401 (2012).
- [5] H. Takatsu, J. J. Ishikawa, S. Yonezawa, H. Yoshino, T. Shishidou, T. Oguchi, K. Murata, and Y. Maeno, *Phys. Rev. Lett.* **111**, 056601 (2013).
- [6] N. Kikugawa, P. Goswami, A. Kiswandhi, E. S. Choi, D. Graf, R. E. Baumbach, J. S. Brooks, K. Sugii, Y. Iida, M. Nishio, S. Uji, T. Terashima, P. M. C. Rourke, N. E. Hussey, H. Takatsu, S. Yonezawa, Y. Maeno, and L. Balicas, *Nat. Commun.* **7**, 10903 (2016).
- [7] P. J. W. Moll, P. Kushwaha, N. Nandi, B. Schmidt, and A. P. Mackenzie, *Science* **351**, 1061 (2016).
- [8] K. P. Ong, D. J. Singh, and P. Wu, *Phys. Rev. Lett.* **104**, 176601 (2010).
- [9] M. E. Gruner, U. Eckern, and R. Pentcheva, *Phys. Rev. B* **92**, 235140 (2015).
- [10] H. J. Goldsmid, *J. Electron. Mater.* **40**, 1254 (2011).
- [11] H. Lengfellner, S. Zeuner, W. Prettl, and K. F. Renk, *Europhys. Lett.* **25**, 375 (1994).
- [12] H. Takatsu, S. Yonezawa, S. Mouri, S. Nakatsuji, K. Tanaka, and Y. Maeno, *J. Phys. Soc. Jpn.* **76**, 104701 (2007).
- [13] H. Yagi, W.-S. Seo, and K. Koumoto, *Key Eng. Mater.* **181–182**, 63 (2000).
- [14] T. Harada, K. Fujiwara, and A. Tsukazaki, *APL Mater.* **6**, 046107 (2018).
- [15] See Supplemental Material at <http://link.aps.org/supplemental/10.1103/PhysRevMaterials.3.085403> for correction procedure to resistivity  $\rho(T)$  and Seebeck coefficient  $S(T)$  data in PdCoO<sub>2</sub> thin films deposited on Al<sub>2</sub>O<sub>3</sub> (0001) offcut substrates.
- [16] G. Yao, M. Gao, Y. Ji, W. Liang, L. Gao, S. Zheng, Y. Wang, B. Pang, Y. B. Chen, H. Zeng, H. Li, Z. Wang, J. Liu, C. Chen, and Y. Lin, *Sci. Rep.* **6**, 34683 (2016).
- [17] K. Yoshida, Y. Maeno, S. Nishizaki, S. Ikeda, and T. Fujita, *J. Low Temp. Phys.* **105**, 1593 (1996).
- [18] I. Terasaki, Y. Sasago, and K. Uchinokura, *Phys. Rev. B* **56**, R12685(R) (1997).
- [19] S. Ghannadzadeh, S. Licciardello, S. Arsenijević, P. Robinson, H. Takatsu, M. I. Katsnelson, and N. E. Hussey, *Nat. Commun.* **8**, 15001 (2017).
- [20] O. Gunnarsson, M. Calandra, and J. E. Han, *Rev. Mod. Phys.* **75**, 1085 (2003).
- [21] J. Merino and R. H. McKenzie, *Phys. Rev. B* **61**, 7996 (2000).
- [22] X. Deng, J. Mravlje, R. Žitko, M. Ferrero, G. Kotliar, and A. Georges, *Phys. Rev. Lett.* **110**, 086401 (2013).